Analysis of broken rotor bars in large induction motors

Cleber Gustavo Dias[1],
Ivan Eduardo Chabu[2]
[1]Uninove; [2]PEA-USP. São Paulo – SP [Brasil]
diascg@ig.com.br

A new technique to detect broken rotor bars, in large squirrel-cage induction motors is presented. In order to avoid problems in industrial applications, the electromagnetic behavior of induction machines with rotor faults was examined, by using a mathematical model. Simulation results are presented from the model implemented in the Simulink-Matlab. Experimental results are presented in order to validate the proposed method.

Key words: Broken bars. Diagnostic system. Fault analysis. Induction motor.

1 Introduction

The study on induction motor behavior has become fundamental in order to avoid production losses, in industrial applications. Three-phase squirrel-cage induction motors are widely used in industrial plants. Nowadays, it is very important to know the operational conditions of an induction motor in real time, to reduce still, unexpected failures, downtime and operational costs.

During the operation of an induction motor, many types of faults can be avoided, involving electrical and mechanical faults. A rotor failure is related to 10% of total faults in an induction machine (THOMSON; FENGER, 2001). A rotor failure doesn't cause immediate problems, however this kind of fault can produce serious secondary effects, like mechanical vibrations, temperature rise, or damage to the stator core and windings, in a relatively short period (PENMAN; STAVROU, 1996).

A rotor cage fault can be detected before its installation (DOBRODEYEV et al., 2000), however, in industrial applications, it is very important to detect incipient faults, aiming to avoid severe operational conditions. During the last years, many researchers have demonstrated interest in developing techniques to identify bar failure in an induction motor. In the early 1970s, a generalized rotating field theory was used to show that asymmetries appear in the stator and rotor, when a fault occurs.

The rotating-field theory to describe a rotor fault based in a mesh model was used (WILLIAMSON; SMITH, 1982). That work assumes that the rotor bars are insulated from rotor iron. It is shown later (WALLISER; LANDY, 1992) that, inter bar currents reduce the magnitude of any additional stator current sidebands, caused by a broken rotor bar, making difficult its detection.

In Siyambalapitiya, McLaren and Acarnley (1987), a rotor cage monitoring system, using direct temperature measurement, is applied to identify a rotor fault in a large induction motor. However, it is necessary to use a large number of measuring points, otherwise, the measured signals could suggest, for example, an overload.

In Cho, Lang and Umans (1992), a variety of sensors is used to detect broken rotor bars. The sensors measure stator voltage, stator current, stator excitation frequency, and rotor speed. The rotor resistance is estimated and compared to its nominal value to detect broken rotor bars.

Another works showed later that it was possible to detect the existence of broken bars, by examining the stator current spectrum (KLIMAN et al., 1988). Those works (WILLIAMSON; SMITH, 1982; KLIMAN et al., 1988; THOMSON, 1992; BELLINI et al., 2002; THOMSON; FENGER, 2003) still showed that a broken bar results in current components being induced in the stator winding at frequencies given by:

$$fsb = f1(1\pm2s)Hz \quad (1)$$

Where:

fsb = frequencies of sidebands due to broken rotor bars, Hz;

f1 = supply frequency, Hz;

s = per unit slip of the induction motor.

In Thomson (1992), it's shown the influence of mechanical loads and rotor design on the diagnosis of broken rotor bars, using current spectrum. A mathematical model of the induction machine was made (TOLIYAT; LIPO, 1995; LUO et al., 1995; FISER; FERKOLJ, 1996; MANOLAS; TEGOPOULOS; PAPADOPOULOS, 1996) to study the motor behavior with rotor faults. In Fiser and Ferkolj (1998), the finite ele-

ment method is used in research of the magnetic field of induction motor with rotor cage asymmetry due to a broken rotor bar.

In Milimonfare and collaborators (1999), a new approach was proposed to detect broken rotor bars. The motor is disconnected from the supply, and the induced voltage in the stator, due only to the rotor flux is utilized to detect the fault. Recently, in Benbouzid and Kliman (2003), Henao, Demian and Capolino (2003) and Demian and collaborators (2004), some techniques have been presented for the detection of broken bars and bearing deterioration in induction motors, like current spectrum, stator current and power spectra, high resolution spectral analysis, wavelet analysis, Park's Vector Approach and Adaptive Statistical Time-Frequency Method.

The aim of this paper is to present a new technique to detect broken bars in large induction motors. As shown by Figure 1, the method is based on monitoring the magnetic flux density near the rotor bars that usually are slightly extended outside the rotor core in those machines.

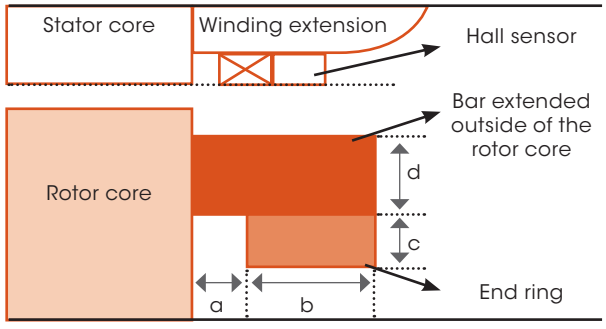

Figure 1: Rotor bar extended outside the rotor core

Source: The author.

The leakage flux created by the rotor currents is measured by a Hall effect sensor, installed near the rotor bars. The sensor will be able to detect a single broken bar, by observation of the resulting magnetic flux variation, caused by the failure. It is possible to detect one broken bar, before occurring other faults.

2 Mathematical modeling of the proposed method

This paper suggests a method to detect a broken bar in a squirrel-cage rotor, which consists in evaluation of the resulting magnetic flux density, in a Hall effect sensor, as shown in Figure 2.

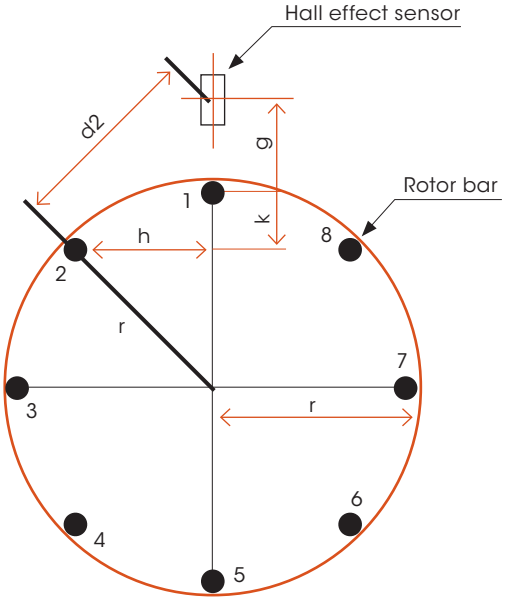

Figure 2: A squirrel-cage rotor with eight bars

Source: The author.

In this case, each bar contributes in a resulting magnetic flux density, by its leakage flux. When a fault occurs, like a broken bar, the flux density pattern changes and it can be detected, by monitoring the resulting flux variation in the sensor.

As shown in Figure 3, the Biot Savart's law was used to identify the magnetic field intensity, produced by each bar.

The Biot Savart's law can be written as follows:

$$h = \oint \frac{i}{4\pi} \frac{\vec{dl} \cdot \vec{r}}{|\vec{r}|3} \quad (2)$$

Equation 2 allows giving the magnetic field intensity in point P, by current flowing in the conductor. In this paper, the conductor is a rotor bar. The magnetic flux density can be obtained using (3), as follows:

$$B = \mu_0 H \quad (3)$$

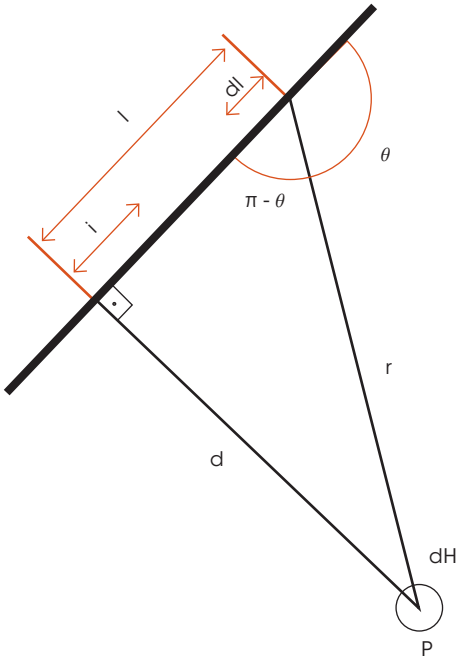

Figure 3: Biot Savart's law applied in a conductor
Source: The author.

Replacing (2) in (3),

$$B = \int_{dl=-\infty}^{dl=+\infty} \frac{\mu_0 i}{4\pi} \quad (4)$$

The vector r can be written as,

$$r = \sqrt{l^2 + d^2} \quad (5)$$

The angle between r and dl vectors can be calculated by equation 6, as follows:

$$\text{sen}\theta = \text{sen}(\pi - \theta) = \frac{d}{\sqrt{l^2 + d^2}} \quad (6)$$

Replacing (6) in (4),

$$B = \frac{\mu_0 i}{4\pi} \int_{-\infty}^{+\infty} \frac{d \cdot dl}{(l^2 + d^2)^{\frac{3}{2}}} \quad (7)$$

Solving (7) for B, in a linear conductor,

$$B = \frac{\mu_0 i}{2\pi d} \quad (8)$$

The resulting magnetic flux density can be obtained by applying (8) for each bar, that is, in each period of time, the magnetic flux density can be calculated using i and r, for the respective bar. For this paper, it is assumed that $d = d_n$. Throughout the calculus, the distance between each bar and the sensor is obtained using (9), as follows:

$$d_n = \sqrt{K^2 + L^2} \quad (9)$$

Where:

$$K = \{R \cdot \text{sin}[\beta_n + (n - 1)\,\lambda]\} \quad (10)$$

$$L = \{g + R[1 - \cos(\beta_n + (n-1)\,\lambda)]\} \quad (11)$$

d_n =distance between nth bar and sensor;
R = rotor radius;
g = minimum distance between sensor and a bar center;
n = number of rotor bars;
β_n = angle between nth bar and sensor axis;
λ = angle between two adjacent bars.

The resulting magnetic flux density in the sensor is obtained for each bar, using (12), as follows:

$$B = \frac{\mu_0}{2\pi} \sum_{1}^{n} \left(\frac{i_n}{d_n}\right) \cos\alpha_n \qquad (12)$$

Where:

i_n = electric current flowing in the nth bar;

$\cos\alpha_n$ = angle used to calculate the contribution in the sensor for each bar.

The electric current flowing in each bar was calculated using (13), as follows:

$$i_n = I_m \cdot \sin[(\omega_s - \omega_r) \cdot t - (n - 1)\,\lambda] \cdot p \qquad (13)$$

Where:

t = time;

I_m = maximum current;

ω_s = synchronous angular speed;

ω_r = rotor angular speed.

3 Simulation results

In this paper the mathematical model based in (9), (12) and (13) was implemented in the Simulink-Matlab tool. The model was simulated for both healthy and faulted rotors. For simulation purposes the parameters were used as shown in the Table 1, from a hypothetical induction motor. In Figure 4, it is possible to observe the resulting magnetic field density on a Hall effect sensor, obtained for a healthy motor, without broken rotor bars. In Figure 5 it's shown a simulation with two broken rotor bars. During the simulation, a resulting magnetic field density variation has been noticed, mainly when the broken bars were near the sensor. In Figure 6 it is possible to observe the failure in more detail. For a fault simulation, the broken bar current is set to zero in the Matlab model.

Table 1: Parameters used in the simulation

Parameter	Value
Rotor diameter	0.4 m
Rotor bars	80
Number of poles	4
Distance between sensor and point A (g)	0.012 m
Rotor bar current (RMS)	400 A
Supply frequency	60 Hz
Slip	2%

Source: The author.

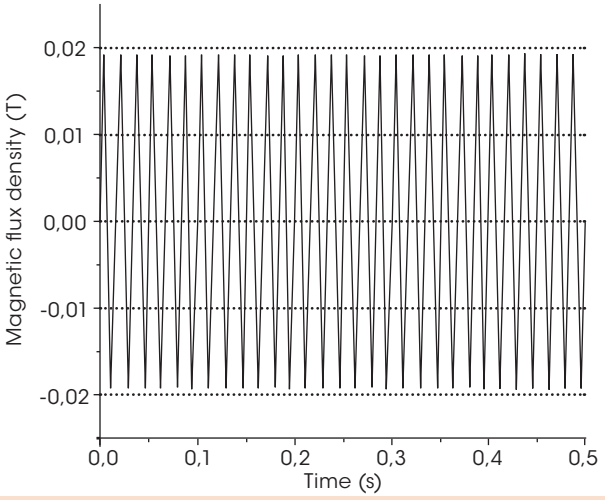

Figure 4: Resulting magnetic field density for a healthy motor

Source: The author.

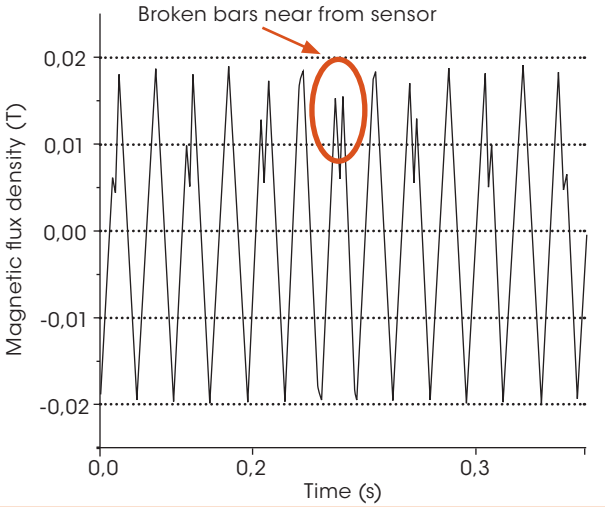

Figure 5: Resulting magnetic field density for a faulted rotor

Source: The author.

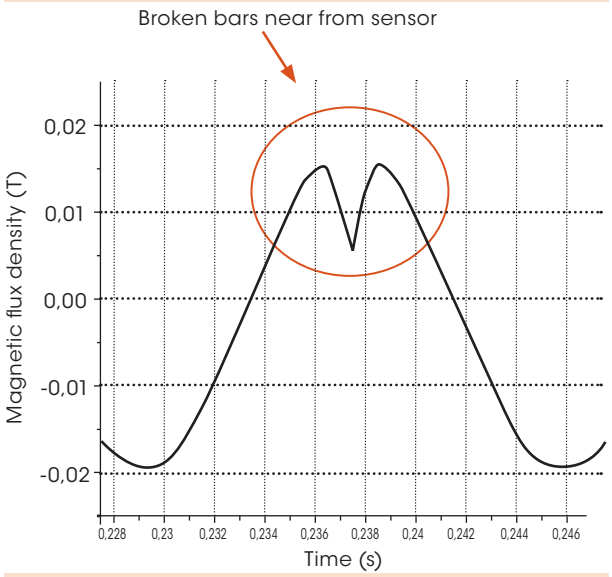

Figure 6: Resulting magnetic field density for a faulted rotor (two broken bars) in details

Source: The author.

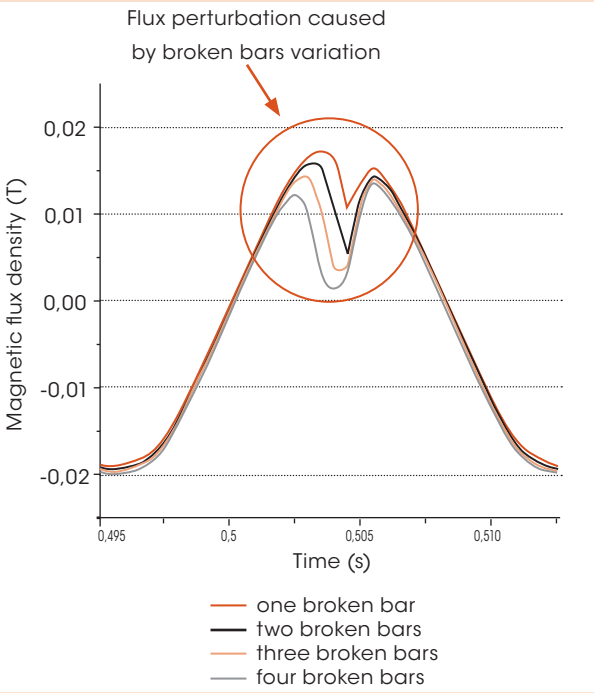

Figure 7: A comparison between four cases involving one, two, three and four broken rotor bars

Source: The author.

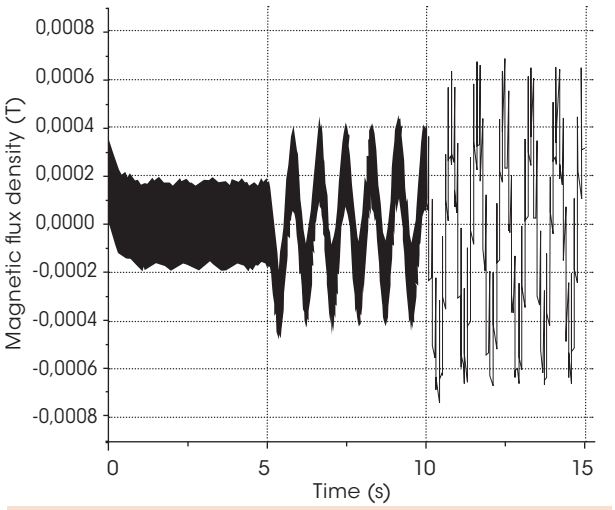

Figure 8: Resulting magnetic flux density filtered on the slip frequency

Source: The author.

The Figure 7 shows a comparison between three situations: one, two, three and four broken rotor bars. In this case, it was noticed that when the number of broken bars increases, there is a larger variation in the resulting magnetic field density in the sensor.

Using a Butterworth low pass filter on the slip frequency during the simulation, it was possible to observe that the resulting magnetic field density varies on the slip frequency when a fault occurs, as shown in Figure 8.

The Figure 8 shows a simulation involving one (t = 5 s) and two (t = 10s) broken bars, however, the resulting magnetic flux density was filtered on the slip frequency (s = 2%). According the results, a filter can be used to help on the fault detection.

A spectral analysis of the magnetic flux density (B), proves that the signs varies on the slip frequency (s = 2%), when a fault occurs, as shown by Figure 9. In that case, it was made a simulation with 10 broken bars, due to its magnitude. It is important to explain that the spectral analysis was used just to show that the fault varies on the slip frequency, but the proposed method is based on the observation of the valley caused by broken bars, when they are near from Hall effect sensor. The width and depth of the valley indicate the fault gravity.

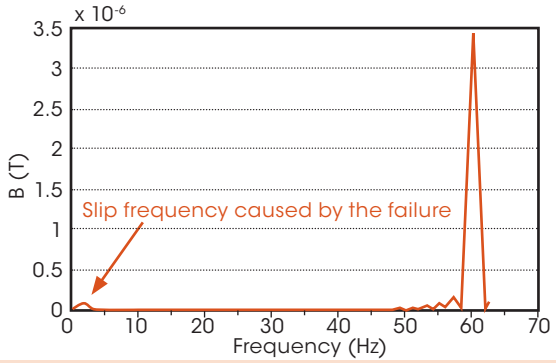

Figure 9: Spectral analysis of the resulting magnetic flux density for a faulted rotor (ten broken bars)

Source: The author.

4 Experimental results

In order to validate the mathematical model, experimental tests were made. The Figure 10 shows the installation of the Hall effect sensor between two stator coils. Its rotor is composed by 58 bars. The resulting magnetic flux density has been measured by a digital oscilloscope connected to the Hall effect sensor. Experimental tests have been made in induction motor with two bars disconnected from its end ring.

It is possible to observe the initial experimental results obtained for a faulted rotor with two broken bars. In this case, it was noticed that the resulting magnetic field density in the sensor has the similar behavior with the simulation results.

The Figure 11 shows a good approach between simulation and experimental results. In this case, it was considered the stator contribution, applying Biot Savart Law for each stator slot current.

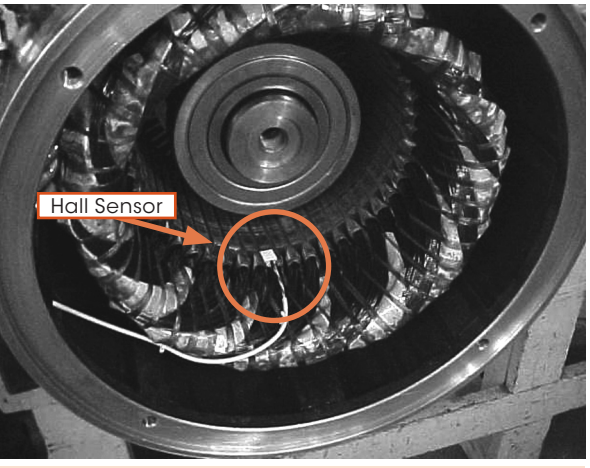

Figure 10: The Hall effect sensor installed between two stator coils

Source: The author.

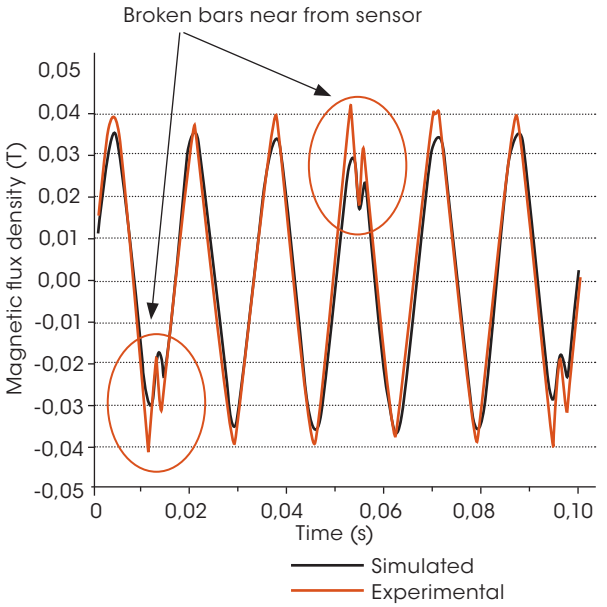

Figure 11: Magnetic flux density variation (valley) on the Hall effect sensor

Source: The author.

In Figure 12 it is possible to observe the magnetic flux density variation in the Hall effect sensor in more details, in the negative cycle.

5 Final considerations

Biot Savart's law was used in this work, in order to identify a broken rotor bar, in large squirrel-cage induction motors during its operation. In an industrial environment, for instance, it is possible to monitor the rotor's conditions efficiently.

By observing the resulting magnetic flux density variation in the Hall effect sensor, it is pos-

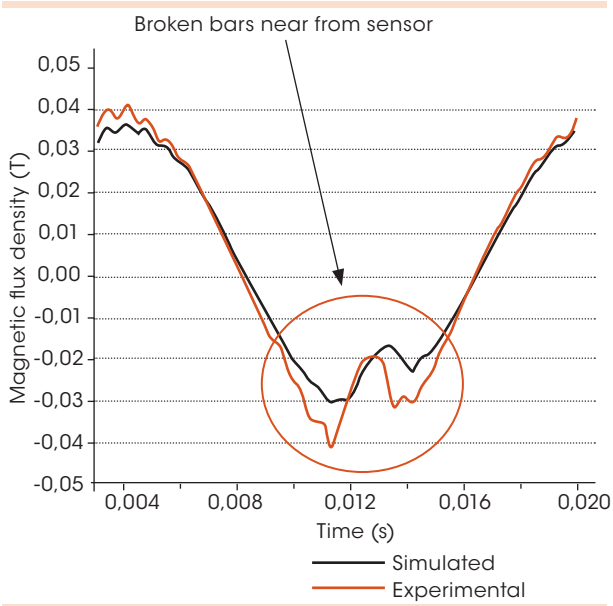

Figure 12: Magnetic flux density variation (valley) on the Hall effect sensor in more details

Source: The author.

sible to detect one broken bar before other broken bars. Experimental results still showed that it was possible to detect two broken bars in a rotor having 58 bars. On the other hand, a method based on stator current spectral analysis will be more difficult to detect broken bars in that case, due to its lower sensitivity.

Extension of this work will be performed involving artificial intelligence techniques and more experimental tests.

References

BELLINI, A. et al. On-field experience with online diagnosis of large induction motors cage failures using MCSA. *IEEE Transactions on Industry Applications*, v. 38, n. 4, p. 1.045-1.053, 2002.

BENBOUZID, M. E. H.; KLIMAN, G. B. What stator current processing-based technique to use for induction motor rotor faults diagnosis? *IEEE Transactions on Energy Conversion*, v. 18, n. 2, p. 238-244, 2003.

CHO, K. R.; LANG, J. H.; UMANS, S. D. Detection of broken rotor bars in induction motors using state and parameter estimation. *IEEE Transactions on Industry Applications*, v. 28, n. 3, p. 702-709, 1992.

DEMIAN, C. et al. Detection of induction machines rotor faults at standstill using signals injection. *IEEE Transactions on Industry Applications*, v. 40, n. 6, p. 1.550-1.559, 2004.

DOBRODEYEV, P. N. et al. Method for detection of broken bars in induction motors. *IEEE Transactions on Magnetics*, v. 36, n. 5, p. 3.608-3.610, sep. 2000.

FISER, R.; FERKOLJ, S. Calculation of magnetic field asymmetry of induction motor with rotor faults. In: MEDITERRANEAN ELECTROTECHNICAL CONFERENCE, 1998, Tel Aviv. *Proceedings*... Tel Aviv: IEEE, 1998. v. 2, p. 1.175-1.179.

FISER, R.; FERKOLJ, S. Modeling of failure states of induction machines, In: MEDITERRANEAN ELECTROTECHNICAL CONFERENCE, 1996, Bari. *Proceedings*... Bari: IEEE, 1996. v. 3, p. 1.195-1.198.

HENAO, H.; DEMIAN, C.; CAPOLINO, G. A. A frequency-domain detection of stator winding faults in induction machines using an external flux sensor. *IEEE Transactions on Industry Applications*, v. 39, n. 5, p. 1.272-1.279, 2003.

KLIMAN, G. B. et al. Noninvasive detection of broken rotor bars in operating induction motors. *IEEE Transactions on Energy Conversion*, v. 3, n. 4, p. 873-879, 1988.

LUO, X. et al. Multiple coupled circuit modeling of induction machines. *IEEE Transactions on Industry Applications*, v. 31, n. 2, p. 311-318, 1995.

MANOLAS, S. G.; TEGOPOULOS, J. A.; PAPADOPOULOS, M. Analysis of squirrel-cage induction motors with broken rotor bars. In: INTERNATIONAL CONFERENCE ON ELECTRICAL MACHINES, 1996, Virgo. *Proceedings*... Virgo: Icem, 1996. v. 3, p. 19-23.

MILIMONFARE, J. et al. A novel approach for broken-rotor-bar detection in cage induction motors. *IEEE Transactions on Industry Applications*, v. 35, n. 5, p. 1.000-1.006, 1999.

PENMAN, J.; STAVROU, A. Broken rotor bars: their effect on the transient performance of induction machines. *IEE Proceedings – Electric Power Applications*, v. 143, n. 6, p. 449-457, 1996.

SIYAMBALAPITIYA, D. J. T; McLAREN, P. G.; ACARNLEY, P. P. A rotor condition monitor for squirrel-cage induction machines. *IEEE Transactions on Industry Applications*, v. IA-23, n. 2, p. 334-340, 1987.

THOMSON, W. T. On-line current monitoring: the influence on mechanical load or an unique design on the diagnosis of broken bars in induction motors.. In: INTERNATIONAL CONFERENCE ON ELECTRICAL MACHINES, 1992, Manchester. *Proceedings*... Manchester: Icem, 1992. v. 3, p. 1.236-1.240.

THOMSON, W. T.; FENGER, M. Case histories of current signature analysis to detect faults in induction motor drives. In: INTERNATIONAL ELECTRIC MACHINES AND DRIVES CONFERENCE, 2003, Madison. *Proceedings*... Madison: 2003. v. 3, n. 1-4, p. 1.459-1.465.

THOMSON, W. T.; FENGER, M. Current signature analysis to detect induction motor faults. *IEEE Industry Applications Magazine*, v. 7, n. 4, p. 26-34, 2001.

TOLIYAT, H. A.; LIPO, T. A. Transient analysis of cage induction machines under stator, rotor bar and end-ring faults. *IEEE Transactions on Energy Conversion*, v. 10, n. 2, p. 241-247, 1995.

WALLISER, R. F.; LANDY, C. F. The influence of interbar currents on the detection of broken rotor bars. In: INTERNATIONAL CONFERENCE ON ELECTRICAL MACHINES, 1992, *Proceedings*... Manchester, 1992. v. 3, p. 1.246-1.250.

WILLIAMSON, S.; SMITH, A. C. Steady-state analysis of 3-phase cage motors with rotor-bar and end-ring faults. *IEE Proceedings B – Electric Power Applications*, v. 129, n. 3, p. 93-100, 1982.

Recebido em 18 set. 2006 / aprovado em 20 nov. 2006

Para referenciar este texto

DIAS, C. G.; CHABU, I. E. Analysis of broken rotor bars in large induction motors. *Exacta*, São Paulo, v. 4, n. 2, p. 407-415, jul./dez. 2006.